THE HYDRO-ELASTIC BEHAVIOUR OF FLEXIBLE PANELS WITH INHOMOGENEOUS MATERIAL PROPERTIES AND ADDED RESTRAINTS

M W Pitman and **A D Lucey,** Curtin University of Technology, Australia

SUMMARY

This paper presents the application of new approach that is a hybrid of theoretical and computational methods in the linear-stability analysis of elastic plates subject to infinite Reynolds-number fluid loading over one side. The method permits the extraction of system eigenvalues and eigenmodes for the fully coupled Fluid-Structure Interaction (FSI) system for complex configurations that are not amenable to the methods of conventional theoretical analysis. The panel configurations studied in this case involve plates with multiple hinge joints along their length and plates with spatially varying properties. Results indicate that such complex boundary conditions strongly influence the stability of the panel. These results have important implications for the use of material inhomogeneity and additional constraints to postpone the hydro-elastic instability of flexible panels on ship hulls or for the use of compliant panels in drag-reduction strategies.

~~~~~~

1. INTRODUCTION

The stability of a one-sided flexible panel interacting with potential flow is perhaps the most fundamental problem in Fluid-Structure Interaction (FSI). The deceptively subtle dynamics of this system have practical implications ranging from the structural integrity of high-speed ship hulls to drag reduction with the use of compliant walls. This paper focuses on the prediction of flow-induced instabilities, divergence (buckling) or flutter, of such panels that can be a limiting factor in the design of light but durable ship hulls.

A schematic of the FSI system studied is presented in Figure 1. The system is modelled as two-dimensional flexible panel interacting with a flow of very high, actually infinite, Reynolds number. The panel may be held at each end through a variety of boundary conditions such as clamped, hinged or free (unrestrained). However, in this study the hinged boundary condition is applied to each end. The effects of energy dissipation through material damping are included through the addition of distributed dash-pot damping on the underside of the panel.

The hydroelastic stability of the system represented by Figure 1 has a long history of study; see, for example, Djugundi *et al.* [4], Weaver & Unny [14], Ellen [5], Garrad & Carpenter [7], and Lucey & Carpenter [10]. All such studies predict that there exists a critical flow speed at which the panel succumbs to divergence instability that is replaced by panel flutter when the flow speed is increased further. The Galerkin method is most often used to obtain the solution of the FSI system. For this to be a practicable strategy requires that relatively simple restraints are used and that a panel of homogeneous construction is modelled.

In this paper we briefly describe and then apply the new approach of Pitman & Lucey [12] for analysing the linear-stability of finite fluid-structure systems. The power of the method lies in the ability to extract eigenvalues and eigenmodes from the complete FSI system even when the elastic plate has 'non-standard' properties. The flexible panel may be modelled with arbitrary inhomogeneity in its material properties and/or with multiple complex boundary conditions for which it would be difficult, or perhaps impossible, to resolve the system eigenvalues and eigenmodes using conventional theoretical analysis.

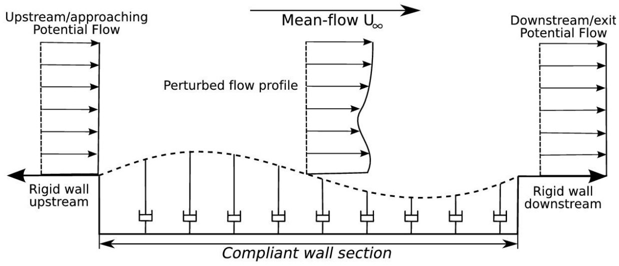

Figure 1: Schematic of the fluid-structure system that comprises an inviscid flow (infinite Reynolds number or 'potential') over a flexible panel.

2. SYSTEM EQUATION

The motion of the flexible panel is modelled by the linear two-dimensional beam equation with an extra term added to account for uniform dashpot-type damping to represent any energy dissipation in the material. Motion is forced by perturbations from the mean fluid pressure Wall motion is therefore governed by

$$\rho_m h \frac{\partial^2 \eta}{\partial t^2} + d\frac{\partial \eta}{\partial t} + B\frac{\partial^4 \eta}{\partial x^4} = -\Delta p(x,0,t) \ , \qquad (1)$$

where $\eta(x,t)$, ρ_m, h and B are respectively, the plate's deflection, density, thickness and flexural rigidity, while $\Delta p(x,y,t)$ is the fluid pressure perturbation from the undisturbed mean-flow value. In the present problem we apply hinged-edge conditions at the leading and trailing
~~~~~~

edges of the plate although there is no necessary restriction on such boundary conditions in the method that follows.

The fluid is modelled as incompressible and irrotational. This is an appropriate approximation of the essentially potential flow outside the boundary layer. Rotationality and viscous effects of the boundary layer are ignored which implies that the boundary layer is thin with respect to the wall disturbance wavelength and amplitude and thus the Reynolds number is very high (infinite). This is a reasonable modelling approximation for many high-speed marine applications. However, in Section 5.3 below, we describe how the present method can be extended to incorporate boundary-layer effects.

A velocity perturbation potential $\phi(x,y,t)$, that satisfies Laplace's equation and the kinematic condition of no fluid flux through the solid-fluid interface

$$\frac{\partial \phi}{\partial y} = \frac{\partial \eta}{\partial t} + U_\infty \frac{\partial \eta}{\partial x} \quad , \tag{2}$$

and the far-field condition is introduced. This solution is then used in the linearised unsteady Bernoulli equation

$$\Delta p = -\rho \frac{\partial \phi}{\partial t} - \rho U_\infty \frac{\partial \phi}{\partial x} \quad , \tag{3}$$

where ρ and U_∞ are, respectively, the fluid density and flow speed to obtain the perturbation pressure.

The result of Equation 3 can then be substituted into the right-hand side of Equation 1 to generate the system equation.

3. SOLUTION OF SYSTEM EQUATION

3.1 EXISITING METHODS

The solution to the system represented by Equations 1, 2 and 3 has been achieved previously. The classical boundary-value approach determines the long-time solution usually by means of a Galerkin method. The system solution is constructed using the combination of a finite set of *in-vacuo* eigenmodes of the flexible wall. Examples of this approach may be found in Djugundi *et al.* [4], Weaver & Unny [14], Ellen [5], Garrad & Carpenter [7], and Lucey & Carpenter [10]. However, this approach is not well suited to the analysis of complex panels with inhomogeneous properties and/or complex boundary conditions because obtaining the necessary set of analytic orthogonal functions from which to construct the solution can be difficult.

In contrast the explicit time-marching scheme of Lucey & Carpenter [11] gives a direct numerical solution for the position of the wall throughout time and yields results similar to that of a physical experiment where the position of the wall is photographed or measured (in some way) at finite intervals. This approach replicates the physics of the system and its response to some form of initial excitation. However, it remains a difficult task to post-process the vast amount of information (wall position at all snapshot times). Furthermore, the results contain a mixture of complex transient dynamics which makes the task of extracting information about specific vibration more difficult. However, this approach does reveal information relating to transient behaviour for which the method presented in this paper is not suited.

The method presented here adopts a computational approach to the domain discretisation and solution of Laplace's equation, akin to that of Lucey & Carpenter [11]. A solution methodology is then used which works over the resulting large set of equations, treating them in a similar manner to the Galerkin approach. Thus, the method is a hybrid of existing, well-established computational and theoretical methods.

3.2 THE NEW METHOD: A HYBRID THEORETICAL-COMPUTATIONAL APPROACH

3.2(a) Computational Formulation

A boundary-element solution for the flow field is expressed as the sum of a mean flow plus a distribution of singularities along the deforming interface. In this case, zero-order linear source(-sink) elements are chosen for the singularities, with the strength of each element denoted $\sigma(x)$. With the discretisation of the compliant surface into N elements, each with constant strength σ_i, the vector of element strengths may be determined through a balance of the normal velocity components at the wall, a discretised equivalent of Equation 2.

$$\{\sigma\} = 2U_\infty [\mathrm{D}_1]\{\eta\} + 2\{\dot{\eta}\} \quad , \tag{4}$$

where $\{\sigma\}$ is a vector of singularity strengths and $[\mathrm{D}_1]$ is a first-order spatial differentiation matrix which yields a vector of the gradients of η in the x-direction when post-multiplied by the vector of node displacements $\{\eta\}$. Curly braces indicate that the enclosed variable is a vector while square braces indicate that the variable is a square matrix. Thus, Equation 4, and those that follow, are written in a form that is amenable to matrix algebra and hence computational manipulation.

3.2(b) Eigen-analysis

The singularity strengths $\{\sigma\}$ determined through Equation 4 are used to evaluate the tangential velocity and perturbation potential for each element of the interface through the use of influence-coefficient matrices. Substitution of Equation 4 into Equation 3 yields an expression for the forcing pressure in terms of just the interfacial displacement giving

$$-\{\Delta p\} = 2\rho U_\infty^2[\mathrm{T}][\mathrm{D}_1]\{\eta\} + 2\rho U_\infty[\mathrm{T}]\{\dot{\eta}\} + 2\rho U_\infty[\mathrm{T}][\Phi]\{\dot{\eta}\} + 2\rho[\Phi]\{\ddot{\eta}\} \quad , \tag{5}$$

where [T] is the matrix of tangential-velocity influence coefficients and [Φ] is the matrix of velocity-potential influence coefficients.

The form of Equation 5 shows that the pressure may be expressed as a function of three terms on the right-hand side. These terms are the hydrodynamic stiffness, the hydrodynamic damping, and the hydrodynamic inertia which are dependent on η, $\dot{\eta}$ and $\ddot{\eta}$ respectively. The solution method for the flow field is described in more detail in Lucey *et al*. [9] wherein expressions for the influence coefficients are listed.

Substitution of Equation 5 into Equation 1, expressed in finite-difference matrix form using *N* material points coincident with the control points used in the boundary-element method, gives

$$\{\ddot{\eta}\} = [\mathrm{E}]\{\dot{\eta}\} + [\mathrm{F}]\{\eta\} \quad , \tag{6}$$

where

$$[\mathrm{E}] = \left(\rho_m h[\mathrm{I}] - 2\rho[\Phi]\right)^{-1} \times \left(2\rho U_\infty[\mathrm{T}] + 2\rho U_\infty[\mathrm{T}][\Phi] - d[\mathrm{I}]\right) \quad ,$$

$$[F] = \left(\rho_m h[\mathrm{I}] + 2\rho[\Phi]\right)^{-1} \times \left(2\rho U_\infty^2[\mathrm{T}][\mathrm{D}_1] - B[\mathrm{D}_4][\Phi] - K[\mathrm{I}]\right) \quad .$$

It can be seen that Equation 6 is simply a set of *N* coupled, second-order, differential equations. The *N*×*N* system of second-order equations may be transformed to a set of *2N*×*2N* first-order equations of the form

$$\{\dot{w}\} = [\mathrm{H}]\{w\} \quad , \tag{7}$$

where

$$[\mathrm{H}]\{w\} = \begin{bmatrix} 0 & \mathrm{I} \\ -\mathrm{F} & \mathrm{E} \end{bmatrix} \begin{Bmatrix} \{\eta\} \\ \{\dot{\eta}\} \end{Bmatrix} \quad , \tag{8}$$

The solution of steady-state eigenvalue and eigenvectors from such a set of first-order differential equations is well documented. An assumption is made that the steady state response of the complete system is a linear superposition of eigenmodes for which all parts of the system move with a complex frequency $s = s_R + is_I$ and therefore the system response is governed by a linear superposition of particular solutions of the form

$$w = We^{st} \quad . \tag{9}$$

We note at this point that the number of boundary elements used to discretise the wall and solve for the flow field (as well as the finite-difference solution for the wall equations) may be large. The results presented in Section 3 below use 200 panels along the wall which yields a set of 400 equations from which to extract the eigenvalues and eigenmodes of Equation 7. To aid the solution, computational methods are used to solve for the eigenvalues and eigenmodes from these large sets of equations. The ARPACK solver library is a set of FORTRAN routines for the extraction of eigenvalues from large sets of equations using Krylov subspace projection methods. This is an efficient means of extracting the eigenvalues of interest from a very large set of equations. The ARPACK solver has been implemented through the EIGS command in the MATLAB software.

4. RESULTS

4.1 DIMENSIONAL CONSIDERATIONS

The first result below, Figure 2, is presented in dimensional form whereas subsequent results are plotted for generality using non-dimensional variables but in exactly the same format. Thus, eigenvalues plots have hull-speed on the abscissa and complex vibration frequency on the ordinate. The dimensional results presented relate approximately to an aluminium plate, with a density of 2600 kg/m^3, a Young's modulus of 58.9 GPa, a length of 1.2m in the stream-wise direction and a thickness of 8mm, held by a hinge joint at each end. These parameters were chosen because they are broadly representative of plating found on the hull of a high-speed marine vehicle. The hull-speed is expressed in m/s.

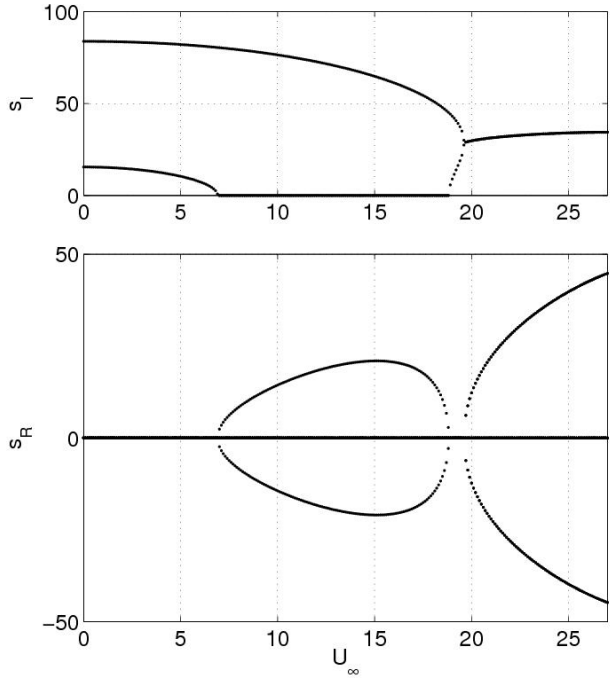

Figure 2: Variation of complex eigenvalues with flow speed for the aluminium plate described in Section 3.1.

Non-dimensional results have been generated using the scheme of Lucey *et al.* [9]; this is appropriate for the

finite system studied here. Accordingly, the hull velocity is replaced with the non-dimensional stiffness ratio,

$$\Lambda^F = \frac{\rho U_\infty^2 L^3}{B} \quad . \tag{10}$$

This is the non-dimensional flow speed for given wall and flow properties. Similarly, time is non-dimensionalised by

$$t' = \left\{ \frac{\sqrt{B/\rho_m h}}{L} \right\} \left(\frac{1}{h} \right) .t \quad . \tag{11}$$

Additionally, for cases where structural damping is introduced, the non-dimensional damping coefficient is,

$$d' = \left(\frac{L^2}{2\pi^2 \sqrt{\rho_m B}} \right) d \quad . \tag{12}$$

The real part of the complex vibration frequency (s_R+is_I) represents growth/decay of the wall and may be converted to real growth at all nodes through

$$\eta = e^{s_R t} \eta_O(t) \ , \tag{13}$$

where $\eta_O(t)$ is the oscillatory component of the motion (particularly vibration frequency) and may be translated to real sinusoidal motion through Euler's formula

$$\eta_O(t) = X e^{i s_I . t} = X_R \cos(s_I t) - X_I \sin(s_I t) \ , \tag{14}$$

where X is the complex amplitude of vibration (the complex eigenvector) at some datum time when t=0 and X_I and X_R are its complex imaginary and real parts respectively.

4.2 SIMPLE ELASTIC PLATE

We first present results for a simple homogeneous elastic plate. The plot of complex eigenvalues with varying flow velocity is presented in Figure 2 and reproduced using non-dimensional variables in Figure 3.

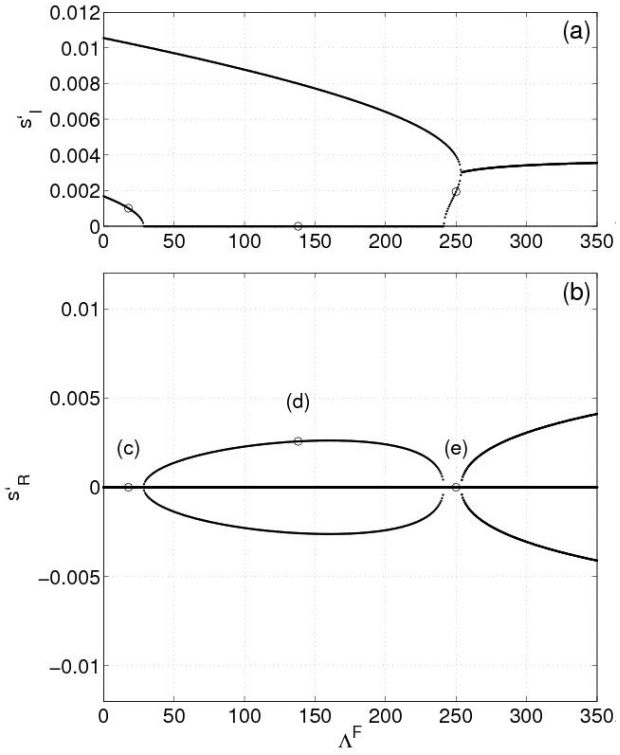

Figure 3: Variation of complex eigenvalues with non-dimensional flow speed for a homogeneous flexible plate; note that this figure is the non-dimensional equivalent of Figure 2.

The solution can be broken into four regions. At low flow speeds the panel is neutrally stable - the eigenvalue has zero real part. However, as the flow speed increases the oscillation frequency, s_I, of the first mode decreases. At the point where Λ^F = 40 (or 7 m/s in Figure 2) the oscillation frequency of the first mode reaches zero and non-zero real part, s_R, of the eigenvalue appears indicating non-oscillatory unstable behaviour. With increasing flow speed, the eigenvalue traces out a 'loop' that closes at approximately Λ^F = 240 (or 18 m/s in Figure 2). This is the divergence range of flow speeds where the plate succumbs to buckling due to the hydrodynamic stiffness component of pressure that creates a force which exceeds the restorative force of the plate. Following the divergence loop, there is a small range of flow speeds in which the plate recovers from instability and becomes neutrally stable (the real part returns to zero). This is the divergence-recovery zone. Finally the plate experiences both unstable (growing) and oscillatory behaviour through first and second mode coalescence. This is a region of strong flutter instability that extends to higher flow speeds where higher modes also participate in the resonance. Typical eigenmodes in the regions of pre-divergence neutrally stable oscillation, divergence instability and neutrally stable post-divergence behaviour, at flow speeds marked respectively by labels (c), (d) and (e) are presented in Figure 4.

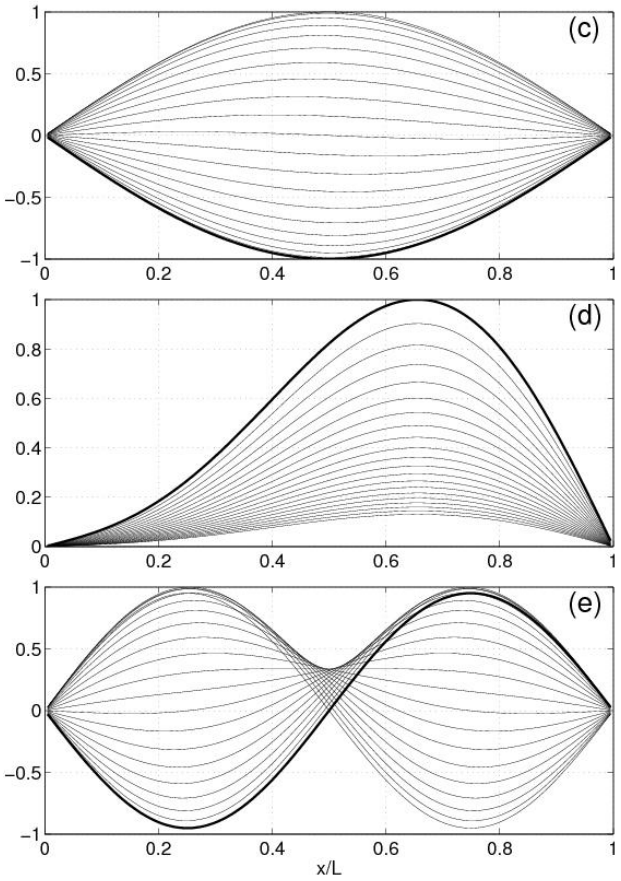

Figure 4: Complex eigenvalues at the different non-dimensional flow speeds marked in Figure 3. The plots depict the shape of the flexible plate through a succession of time steps; the final position for the time period, one cycle of oscillation for cases (c) and (e), is denoted by the thicker line.

4.3 INHOMOGENEOUS FLEXIBLE PLATE

Figure 5 shows the variation of eigenvalues for a flexible wall with properties and configuration identical to the simple elastic plate that generated Figure 3, except that the flexural rigidity of the wall, B, now varies linearly along the length of the wall. However, the mean value of the flexural rigidity B_{ave} is equal to the uniform value of Figure 3 and the non-dimensional flow speed, Λ^F, is based on this value. The gradient of the linear variation is set so that B varies from 1.95 B_{ave} at the upstream edge down to 0.05 B_{ave} at the trailing edge.

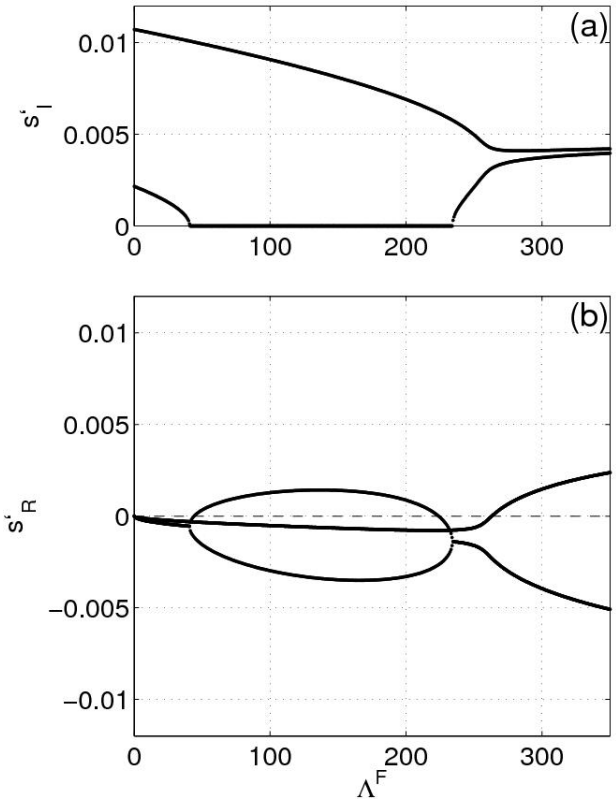

Figure 5: Variation of complex eigenvalues with non-dimensional flow speed for a flexible plate with streamwise varying flexural rigidity.

Qualitatively, the form of the eigenvalues of Figure 5 is similar to Figure 3. However, the linear variation of the plate's flexural rigidity, so that its upstream end is more rigid than its downstream end, moves the divergence loop down and to the right. This indicates that stiffening the upstream half of an elastic plate tends to stabilise the system in a similar manner to the addition of structural damping. Conversely, computations performed with a stiffened downstream end showed that the system was less stable than that of the homogeneous plate with the divergence loop being translated up and to the left.

4.4 ADDED HINGE SUPPORTS

Figure 6 shows results for the same elastic plate as that used for Figure 3 except that an extra hinge constraint has been added at a distance of 0.3L from the upstream edge. Note the increased range of Λ^F values over which the eigenvalues are plotted.

For the fundamental mode, there exists a pre-divergence range where the wall motion is now slightly attenuated. However, the third mode is now found to be unstable in this pre-divergence range. There is then a divergence loop that leads into the modal-coalescence flutter instability with no divergence-recovery zone. The key differences from the behaviour of the simple elastic plate of Figure 3 are: (i) most modes in the pre-divergence range are attenuated, (ii) the system as a whole is more

stable with respect to divergence that sets in at a far higher value of Λ^F, (iii) the absence of divergence-recovery zone of flow speeds, and (iv) a specific mode becomes unstable at low, pre-divergence, values of Λ^F right down to zero flow speed.

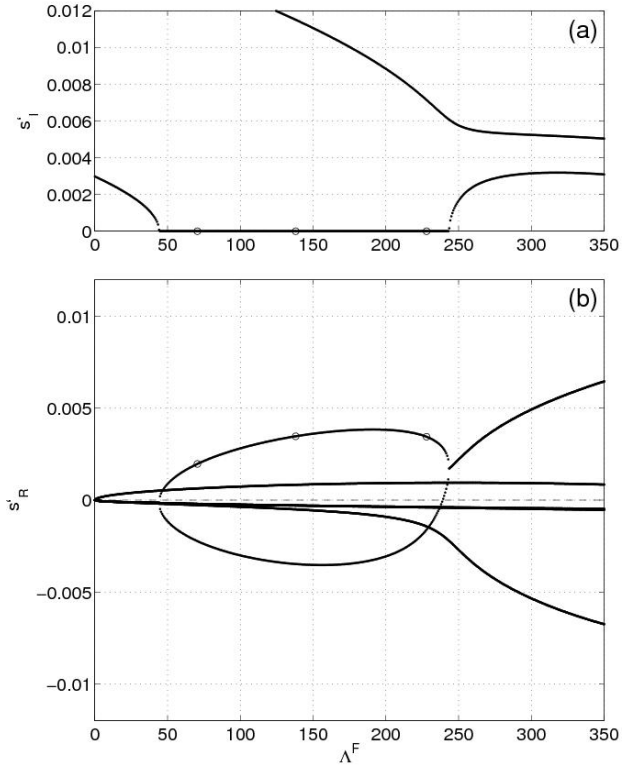

Figure 6: Variation of complex eigenvalues with non-dimensional flow speed for a flexible plate with an added hinge-type restraint at 30% chord length.

The increased stability of the system with respect to divergence could be expected due to the fact that the added hinge joint shortens the effective length of the elastic plate. Basing Λ^F on the length of the longest part of the divided plate places the divergence loop into a similar range of values as seen in Figure 3. However, the critical instability (with increasing flow speed) is now no longer divergence but the new single-mode flutter that exists even in the limit of zero flow speed. This instability principally comprises the third in-vacuo mode. Unlike divergence, it is amenable to control through the action of structural damping. Results not presented here show that, for example, when $d' = 0.082$, the non-dimensional flow speed for its onset is no longer zero but becomes $\Lambda^F = 400$. Thus, in such a case, divergence will then becomes the critical instability with increasing flow speed.

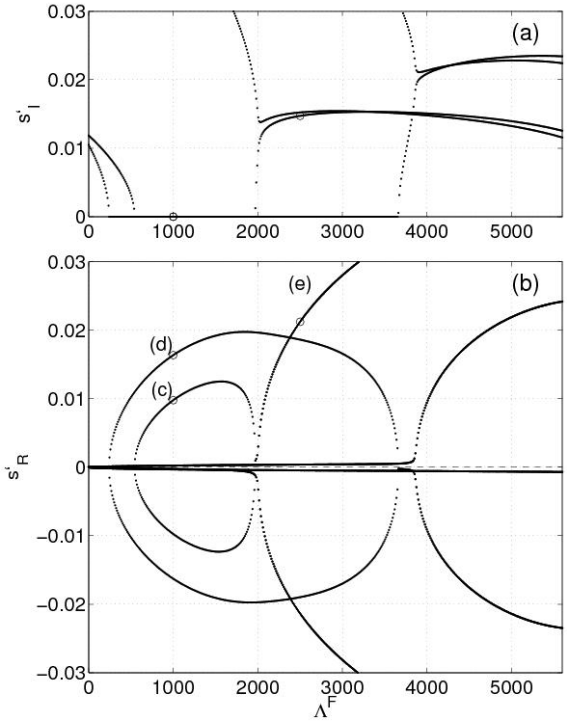

Figure 7: Variation of complex eigenvalues with non-dimensional flow speed for a flexible plate with an added hinge-type restraint at 50% chord length.

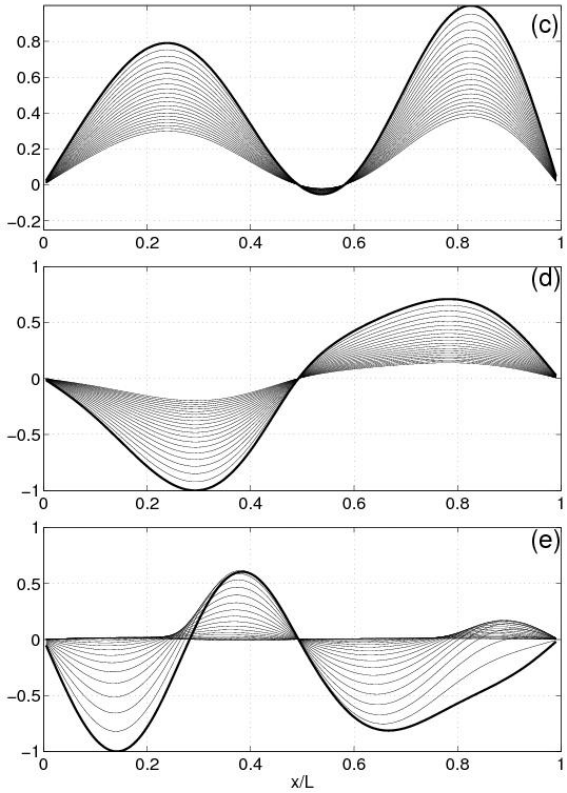

Figure 8: Complex eigenvalues at the different non-dimensional flow speeds marked in Figure 7. The plots depict the shape of the flexible plate through a succession of time steps; the final position for the time period is denoted by the thicker line.

Figure 7 shows results for the same configuration as used to generate Figure 6 except that the additional hinge-joint restraint has been placed at 0.5*L*. The shape of the eigenvalue loci in Figure 7 differs significantly from those in Figures 6 and 3 in that two divergence loops now exist. Figure 8 shows the associated eigenmodes for the inner and outer divergence loops respectively at Λ^F = 1000 and labelled as points (c) and (d) in Figure 7. There are two divergence loops because the addition of the hinge joint at 50% chord introduces further configurations in which instability can occur. Thus, divergence-type instability can occur in either half of the divided panel with each half destabilising in-phase or out-of-phase as seen in Figure 8, plots (c) and (d) respectively. There also exists some weak higher-mode instability at pre-divergence flow speeds down to the limit Λ^F = 0. This is far less severe than the corresponding single-mode flutter predicted in Figure 6 and would most probably be eliminated by the structural damping naturally occurring in the material a real flexible plate.

5. DISCUSSION

The results presented In Section 3 indicate that complex boundary conditions and material properties strongly influence the stability of a flexible panel subject to fluid loading on one side. Different configurations may be used to stabilise or destabilise the elastic plate. These configurations influence the spatially localised energy exchanges between the fluid and structure along the length of the finite flexible panel. A new type of pre-divergence instability is predicted that can arise through the addition of an extra hinge constraint. These results have implications either for the use of material inhomogeneity and additional constraints to postpone hydro-elastic instability of flexible panels on ship hulls or for the use of compliant panels in drag-reduction strategies (for example see Carpenter *et al.* [3]).

5.1 APPLICATION OF RESULTS

In the design of high-speed craft, it is clearly desirable to reduce the unladen weight, and hence the displacement, of the hull in order to reduce the wetted area and thereby reduce skin-friction and, to a lesser extent, wave-making drag. The use of lightweight panels for the hull is a means of achieving this objective. However, such panels must be sufficiently strong to resist both the mean pressure forces that give the ship its buoyancy, and remain free of the hydro-elastic instabilities predicted and discussed in this paper. Concerning the latter requirement, our dimensional results suggest that an aluminium panel of thickness 8 mm and length 1.2m would experience divergence, or bucking, at a ship speed of approximately 13.6 knots (7 m/s). This linear instability would probably saturate at relatively low levels of deformation (Lucey *et al.* [9]) but could result in a mild modification to the fluid-loaded curvature of the hull. For very high ship speeds, Figure 2 indicates that the panel would experience a flutter instability that first sets in at approximately 38.8 knots (20 m/s). This is a dynamic instability that would result in severe structural damage. However, we do recognise that these critical speeds are probably conservative estimates because our analysis is two dimensional. While it is known that the instability mechanisms are primarily two-dimensional, the further restraints along the panel edges have a stabilising influence, as predicted by Lucey & Carpenter [10], the level of stabilisation being dependent upon the aspect ratio of the panel.

5.2 IDENTIFICATION OF NEW INSTABILITY

A new type of instability - single-mode flutter - has been identified in this paper. Ordinarily, the inclusion of further restraints within the streamwise extent of the flexible panel is beneficial because they can postpone divergence and flutter instabilities to higher ship speeds. However, we have shown that they can also trigger this new type of instability which may exist at sub-divergence speeds. While this type of instability is relatively weak, and would probably saturate to low-amplitude limit-cycle oscillations, its presence could have ramifications for the fatigue life of the panel material. Furthermore, the frequency of its oscillation might lead to unwanted acoustic effects. We have shown that this instability can be ‘designed out’ of the hydro-elastic response of the panel through the introduction of structural damping using, for example, material doping.

5.3 BOUNDARY-LAYER EFFECTS

The present modelling has ignored the effect of the intervening boundary layer between the external potential flow and the surface of the flexible wall. Experimental and numerical studies, for example Kendall [8], Balasubramanian & Orszag [1], Gad-el-Hak *et al.* [6], and Carpenter *et al* [2] indicate that the mean shear-layer profile acts to reduce the magnitude of the perturbation-pressure forces. This stabilising effect is strong for laminar boundary layers but far less so for the turbulent boundary layers that occupy most of the streamwise extent of high-speed craft. The new modelling approach can be extended to incorporate such boundary-layer effects. The preliminary work presented by Pitman & Lucey [13] extends the set of system variables from the purely surface-based interfacial deformations to include the strengths of vortex-elements that form the basis for the solution of the linearised Navier-Stokes equations for the flow field. The development of this more complete system model is ongoing.

6. ACKNOWLEDGEMENTS

The authors would like to acknowledge the cooperation of Dr Richard Howell at Warwick University (UK). The work of Kim Klaka and Tim Gourlay at the Centre for

Marine Science Technology (CMST) through collaboration with the Fluid Dynamics Research Group (FDRG) at Curtin University is also acknowledged.

7. REFERENCES

1. BALASUBRAMANIAN, R. & ORSZAG, S.A., 'Numerical studies of laminar and turbulent drag reduction.', *NASA Technical Report*, CHI-57, 1981.

2. CARPENTER, P.W., DAVIES, C. & LUCEY, A.D., 'Hydrodynamics and compliant walls: Does the dolphin have a secret?', *AIAA: Journal of Aircraft*, 38(3), 504-512, 2001.

3. CARPENTER, P.W., LUCEY, A.D. & DAVIES, C., 'Progress on the use of compliant walls for laminar-flow control', *Current Science*, 79(6), 758-765, 2000.

4. DUGUNDJI, J., DOWELL, E. & PERKIN, B., 'Subsonic flutter of panels on a continuous elastic foundation', *AIAA J.*, 1, 1146-1154, 1963.

5. ELLEN, C.H., 'The stability of simply supported rectangular surfaces in uniform subsonic flow.', *Trans. ASME: J. Appl. Mech.*, 40, 68-72, 1973.

6. GAD-EL-HAK, M., BLACKWELDER, R.F. & RILEY, J.J., 'On the interaction of Compliant Coatings with Boundary Layer Flows', *J. Fluid Mech.*, 140, 257-280, 1984.

7. GARRAD, A.D. & CARPENTER, P.W., 'A theoretical investigation of flow-induced instabilities in compliant coatings', *J. Sound Vib.*, 84, 483-500, 1982.

8. KENDALL, J.M., 'The turbulent boundary layer over a wall with progressive surface waves.', *J. Fluid Mech.*, 24, 225, 1970.

9. LUCEY, A.D., CAFOLLA, G.J., CARPENTER, P.W. & YANG, M., 'The nonlinear hydroelastic behaviour of flexible walls.', *J. Fluids Struct.*, 11, 717-744, 1997.

10. LUCEY, A.D. & CARPENTER, P.W., 'On the difference between the hydroelastic instability of infinite and very long compliant panels', *J. Sound Vib.*, 163, 176-181, 1993.

11. LUCEY, A.D. & CARPENTER, P.W., 'A numerical simulation of the interaction of a compliant wall with inviscid flow.', *J. Fluid Mech.*, 234, 121-146, 1992.

12. PITMAN, M.W. & LUCEY, A.D., 'On the direct determination of the eigenmodes of finite flow–structure systems', *Proc. R. Soc. A*, 465, 257–281, 2009.

13. PITMAN, M.W. & LUCEY, A.D., 'Eigen-analysis of a fully viscous boundary-layer interacting with a finite compliant surface', *In Proceedings: 16th Australian Fluid Mechanics Conference*, 2007.

14. WEAVER, D.S. & UNNY, T.S., 'The hydroelastic stbility of a flat plate', *ASME J. Appl. Mech.*, 37, 823-827, 1971.

8. AUTHOR BIOGRAPHIES

Mark Pitman completed his BEng and PhD studies at Curtin University of Technology, after which he took up a post-doctoral position there. He continues to hold a part-time position at the university undertaking research in Fluid-Structure Interaction. He now works as a Senior Engineer in Applied Research at an engineering firm which consults to the building industry.

Anthony Lucey is Professor of Mechanical Engineering at Curtin University of Technology. He took his Bachelor and PhD degrees from Cambridge and Exeter Universities in the UK. Through his career he has held positions in both Industry and Academe. He is an active engineering educator. His principal research areas are Fluid Mechanics and Fluid-Structure Interaction, spanning fundamental to application-focused topics, and from biological to engineered systems.